# Strong, omnidirectional radar backscatter from subwavelength, 3D printed metacubes

Alex W. Powell[1*], John Ware[1], Joseph G. Beadle[1], David Cheadle[2], Tian Hong Loh[2], Alastair P. Hibbins, and J. Roy Sambles[1]

[1]Electromagnetic and Acoustic Materials Group, Department of Physics and Astronomy, University of Exeter EX4 4QL
[2]National Physical Laboratory, Teddington
[*]a.w.powell@exeter.ac.uk

**Metallic metacubes formed of six metal plate faces connected via a metal jack are shown to backscatter microwave radiation extremely powerfully. Experimental radar scattering cross-section (RCS) data from 3D printed samples agrees very well with numerical model predictions, showing a monostatic RCS of fifteen times the geometric cross section. The principal resonance of the metacubes demonstrates near-complete independence of the incident angle or polarisation of the radiation, making the metacube an omnidirectional scatterer. The metacubes are fabricated via additive manufacturing from metal-coated polymer, and are extremely lightweight, making them excellent candidates for improving the radar return signals from small objects such as drones and cubesats.**

## 1. Introduction

.

The world around us from the seas to outer space is becoming crowded with objects that are difficult to detect via conventional radar - from established technologies such as small boats[1] and gliders[2], to new arrivals like quadcopter drones[3], [4] and biscuit-sized cubesats in outer space[5]. The issue of detectability of these new technologies is causing significant problems, such as the shutting down of airports[6] and the loss of dozens of satellites[7], which remain in orbit as dangerous space-junk.

Traditional methods to boost the radar scattering cross-section (RCS) of an object that does not interact strongly with electromagnetic radiation are the addition of a high RCS element such as a corner reflector[8] or a partially coated Luneberg lens[9], [10]. The operation of these RCS-boosting systems is based around the reflection and/or diffraction of microwave radiation, and as such their size must be at least a few wavelengths across in order to ensure efficient operation, and so they are generally rather large (> 20 cm) and heavy[11]. This precludes their use in small or lightweight applications, such as quadcopter drones, which have notoriously small RCS[3], [4], [12] and where a reliable way to boost the detectability remains a significant problem. More recently, several 2D metamaterial retroreflectors have been demonstrated to be effective, achieving comparable results to industry standards,[13]–[15] but these still require a significant surface area, and only operate in a planar configuration and within a limited angular range. What is required is a method to boost the RCS with minimal impacts on the weight and size of the object.

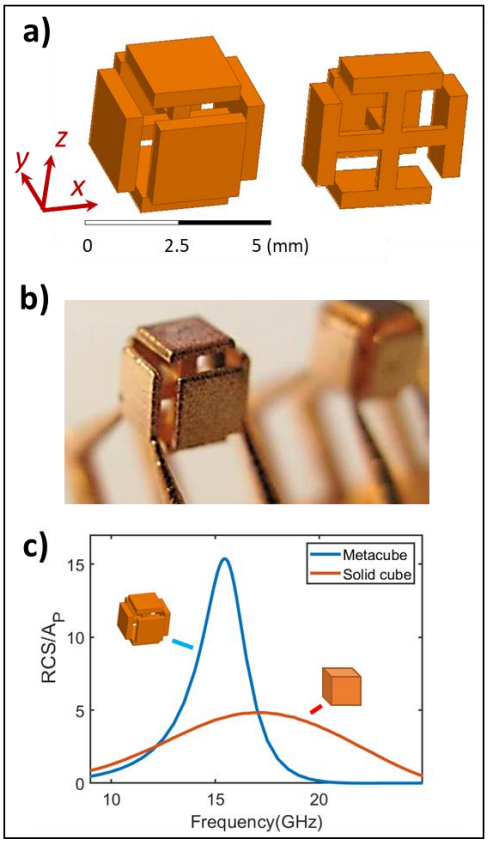


***Figure 1: a)*** *3D diagram of the metacube.* ***b)*** *Metacube samples, 3D printed using a stereolithography printer and then metallised via electroplating.* ***c)*** *The modelled monostatic RCS of a metacube 4.25 mm wide, with a 2.8 mm plate width, a 0.4 mm plate thickness and a 0.8 mm strut support thickness. The monostatic RCS of a 4.25 mm a solid copper cube is also shown, highlighting the increase in RCS caused by the structure of the metacube. Microwave radiation is incident normal to the face of the cube along the x-axis, polarized along the z axis. All RCS values are*

*normalised to the cross sectional area of the cube, $A_P$ =1.8 x $10^{-5}$ $m^2$.*

An alternative to the diffraction-limited systems described above is to utilise subwavelength resonant structures which interact very strongly with incoming radiation and scatter extremely efficiently about a defined resonance, which can be tuned via their geometry. This idea has long been utilised in optics for applications from sensing[16]-[18], to light management in solar cells[16]–[19], but has not been greatly exploited in the microwave regime. In this paper we propose the use of a 3D metacube as a powerful subwavelength scatterer, which shows an RCS profile 15 times its geometric cross section. The cube is effectively constructed of three orthogonal capacitively loaded dipole antennas, and as such shows omnidirectional scattering behaviour, with an RCS that is unchanged at resonance by incident angle and polarisations. We used advanced manufacturing methods such as additive manufacturing via stereolithography and nanocrystalline electroforming to fabricate these complex geometries to a high level of precision, and demonstrate through simulation and experiment the potential of this technique to create 3D omnidirectional superscatterers.

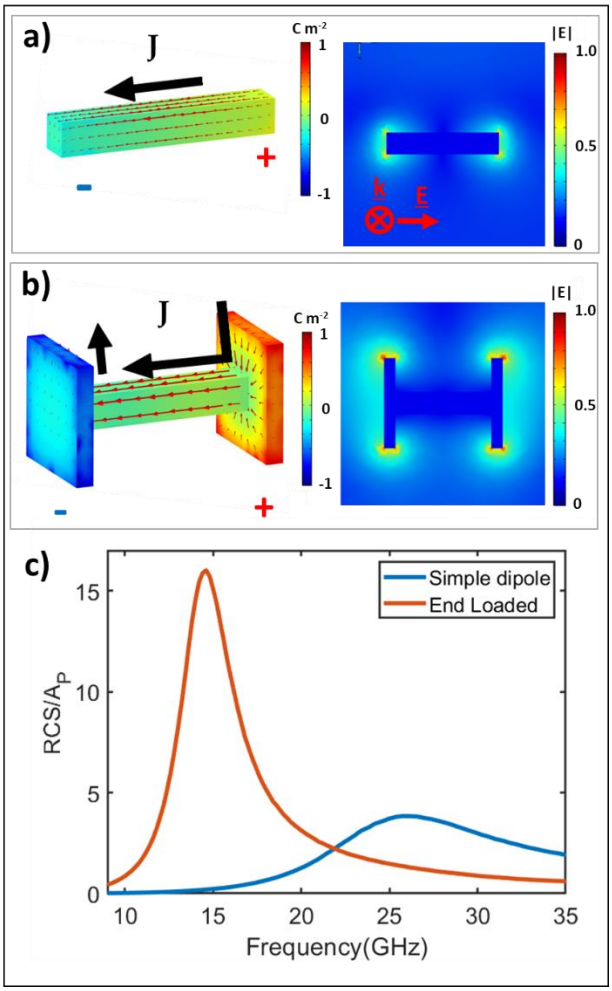


***Figure 2:*** *The surface charge (colouration) and surface current (arrows, left) and the electric field profiles (right) for a simple square rod of length 4.25 mm, and width 0.8 mm at the resonance frequency of 26 GHz* ***(a)*** *and an identical rod terminated with square plates with a plate width of 2.8 mm and a plate thickness of 0.4 mm at 14.6 GHz* ***(b),*** *which is equivalent to one third of the metacube. All values are normalised to the maximum for the plated rods.* ***(c)****The modelled monostatic RCS for both structures (normalised to the cross sectional area of a 4.25 mm cube).*

## 2. Highly scattering subwavelength metacubes

The designed structure of the metacube is shown in Figure 1a. Six metal plate faces are connected via three orthogonal metallic rods, which is labelled here a metal jack. The 3D as-printed and metal-coated structure is shown in Fig. 1b. Visible in this image are the thin connecting supports which held the cubes for printing and coating. The cubes are detached from these for the radar scattering studies reported below. Modelling undertaken using the Comsol RF module, as shown in Fig. 1c this predicts a resonance having a monostatic RCS several times that of a solid copper cube of equivalent cross-section.

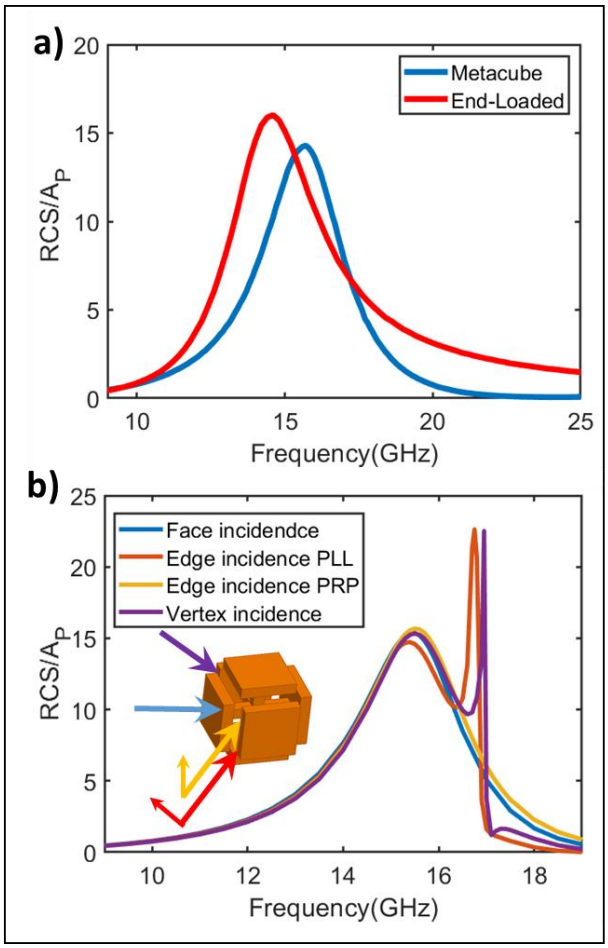


***Figure 3: a)*** *Simulated RCS showing the difference in response between a single, end-loaded dipole (with optimum incident condition) and the 3D metacube.* ***(b)*** *Simulated RCS of the metacube due to microwaves incident along the principle directions with the polarizations indicated (inset). All RCS values are normalised to the cross sectional area of a 4.25 mm cube.*

This enhancement can perhaps be best understood by starting with a single dipole antenna, as shown in Fig. 2a, where the resonance is defined by the dimensions of the rod. The addition of perpendicular metal plates to the ends of the dipole increases the capacitance[20], resulting in a strong redshift of the resonance to lower frequencies. The increase in surface charge (shown in Fig. 2) also leads to stronger electric fields. It also produces greater current flow across the antenna, which will increase the radiation efficiency[21], along with the Q-factor of the antenna[22], as can be seen in Fig. 2c. The Q-factor is raised from $Q$ = 1.9 for the simple dipole to $Q$ =*3.8* for the dipole loaded with two end plates. This simple addition of plates can therefore be said to lead to stronger, narrower, scattering resonances at lower frequencies compared to a simple dipole.

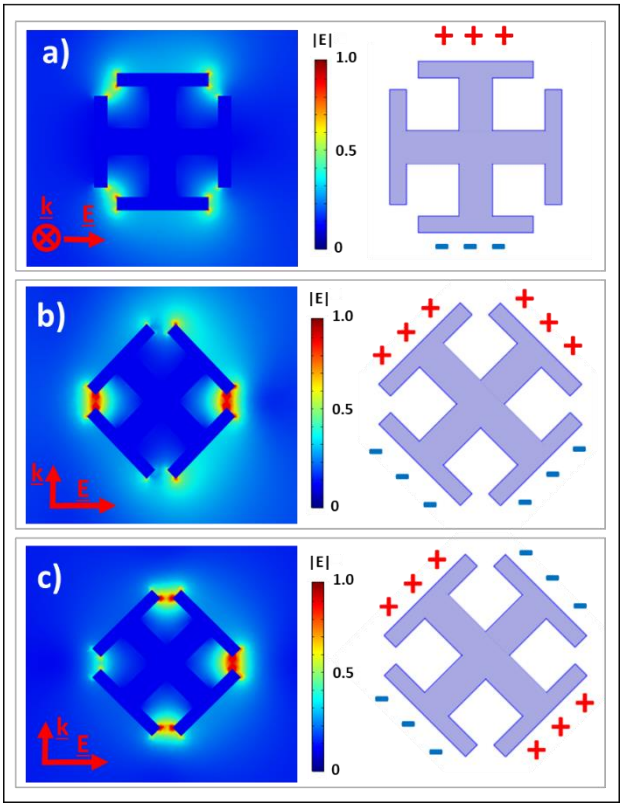


***Figure 4:*** *Simulated electric field plots and charge distribution diagrams of the primary and secondary modes of the metacubes described in Fig. 1, with microwaves incident normal to a face* ***(a)*** *and normal to an edge with perpendicular polarisation* ***(b) & (c)****.*

Whilst this effect is significant, due to the limited symmetry of its geometry, the structure shown in Fig. 2b will only demonstrate this behaviour for selected incident angles and polarizations. Small RCS objects like drones could have any orientation in three-dimensional space and so this very limited angular scope is not particularly useful. To overcome this limitation the metacube shown in Fig. 1a is proposed to achieve omnidirectional scattering behaviour. This is formed of three plate-loaded dipoles at right angles, meaning that for any direction and polarisation the scattering at the dipolar resonance should be the same.

Figure 3a) demonstrates that connecting these three orthogonal plate-loaded dipoles has a small effect on the resonance frequency and Fig. 3b) highlights the omnidirectional scattering behaviour , showing that around the dipolar peak the scattering is almost invariant for all key incident angles and polarisations. For all incident angles, the fundamental mode is an electric dipole at the same frequency, although, due to interaction between the charges on different plates, the electric near-field is substantially different to the normal incidence case (Fig. 4a & 4b). For light incident at an edge and polarised perpendicular to that edge, and light incident along a vertex, a secondary sharp mode is found as shown in Fig. 3b. This is a quadrupolar mode, as demonstrated in Fig. 4c). The rod structures shown in Fig. 2, do not support significant higher order modes, so the mode in Fig. 3b can be said to be a consequence of the 3D structure of the metacube. In this way the metacube is seen to behave like a resonant nanoparticle in the optical, where multiple orders of modes often closely overlap[16], [23] and can lead to very strong forward and reverse scattering[24]. The narrow nature of these quadrupolar resonances could be of interest for applications that must operate in a limited spectral range[25].

It is instructive to take a deeper look into the effect that each geometrical parameter has on the resonances of the metacube. There are four parameters to alter: The length and thickness of the rods, and the width and thickness of the plates. Of these, extending the rod length and the plate width outwards is simply creating a longer dipole and so will result in a redshift of the peaks. The effect of altering the plate widths and rod lengths are less immediately obvious however, and the consequence of a parameter sweep of each is shown in Fig. 5.

It is clear from Fig. 5a that longer plates result in a redshift of the resonance, as well as an increase in RCS magnitude and Q-factor of the peak. This is in alignment with the model of this system (at the fundamental resonance) as a 3D array of capacatively loaded dipoles, where increasing the capping plate length is known to produce the observed effect [23]. Fig 5b also demonstrates adherence of this system to the dipolar model and shows that thinner connecting rods lead to stronger, sharper resonance peaks at longer frequencies.

Therefore it can be said that to achieve the strongest resonance possible for a given size of meta-cube, one must make the plates as large as possible and the connecting rods as thin as possible. However, this will result in a significant narrowing of the resonance, and so for a broadband effect a compromise would have to be determined. Additionally there will always be some trade-offs required to achieve this resonance at a particular frequency, and all parameters will be constrained in practice by the limitations of the method used to fabricate samples.

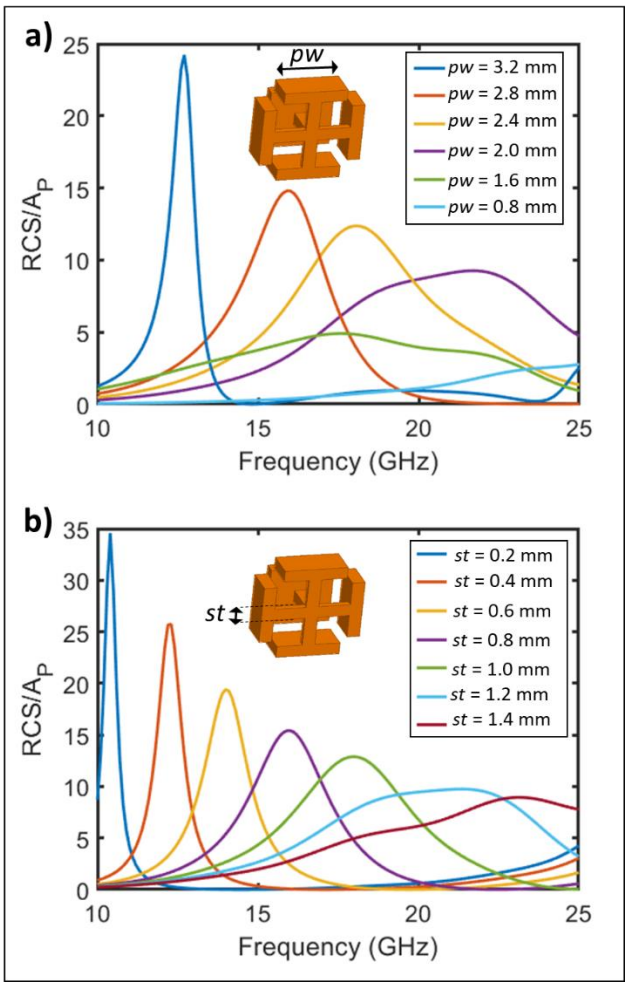


***Figure 5:*** *(a) Simulated effect on the monostatic RCS of changing the plate width, pw, for a metacube 4.25 mm wide, with a 0.4 mm plate thickness and a 0.8 mm strut support thickness. (b) Simulated effect on the monostatic RCS of changing the support thickness, st, for a metacube 4.25 mm wide, with a 2.8 mm plate width and a 0.4 mm plate thickness. Microwave radiation is incident normal to the face of the cube along the x-axis, polarized along the z axis. The insets list the parameter being altered in each case.*

## 3. Experimental Verification

To verify these model results, we fabricated several metacubes via stereolithography 3D printing using a Formlabs Form2. Samples were then coated in a 5 μm layer of copper, ensuring the copper was thick enough to exceed the skin depth at the frequency of interest (around 0.5 μm at 15 GHz). A typical resulting metacube is illustrated in the photograph of Fig. 1b. Its final dimensions were: overall size 4.21 ± 0.04 mm; plate size 2.78 ± 0.05 mm; plate thickness 0.41 ± 0.02 mm; rod width 0.82 ± 0.03 mm. It is worth noting that due to the small quantity of metal used, these samples are very light, weighing 0.042 ± 0.002 g each. Thus even a substantial array would have a negligible impact on the weight of any object they are added to, making them ideal for applications where light weight as well as high radar visibility are critical, such as for quadcopter drones, gliders and cubesats.

The radar cross section (RCS) measurements were carried out in NPL's small antenna radiated testing (SMART) chamber[26]. The chamber has shielded room dimensions of 7.15 m long 6.25 m wide 6.25 m high, whose inner surfaces are fully lined with 45 cm long TDK polyethylene foam pyramidal absorber. A bi-static system with two ETS 3117 horns was used (see Figure 6a). Tests were performed with the metacube positioned at the centre of rotation of the turntable. Brass reference spheres with diameters of 12.7, 8 and 4 mm were measured using the same setup as the metacube to validate the measurement system. The main supports used for the reference sphere and metacube were made with Rohacell 31HF foam, with a base support made from polystyrene blocks. For each measurement an empty chamber trace was taken, with supports in place but the item to be measured absent. Then the metacube was positioned, and a vector network analyser (VNA) was employed to measure the reflected voltage ratio as a complex value where cable losses and VNA isolation was also measured and used to correct the measured voltage ratios. Note that to reduce coupling and crosstalk between the transmitting and receiving horns a small screen was inserted between them.

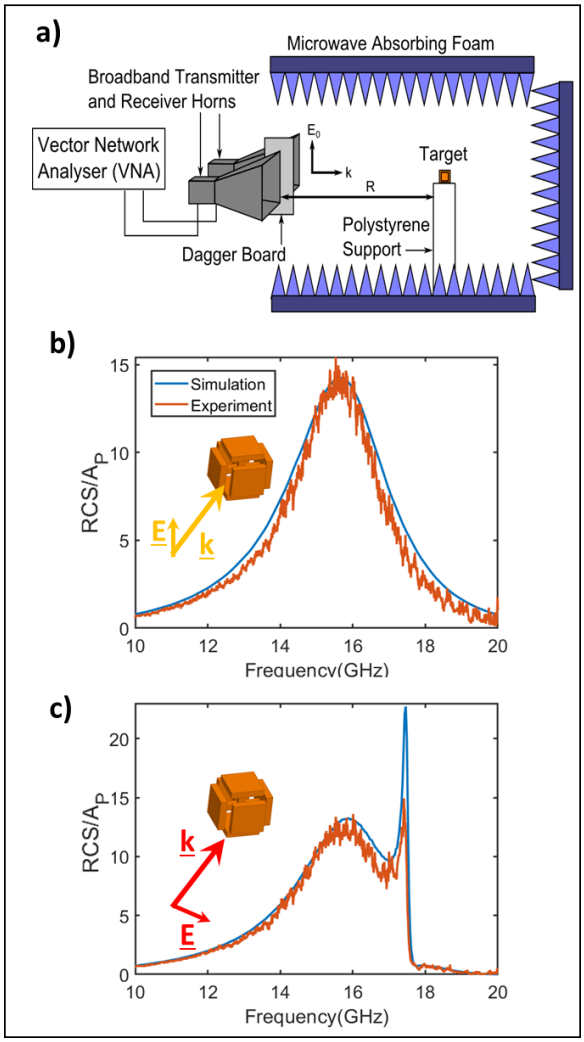


***Figure 6:*** *(a) Experimental setup used to calculate the RCS. (b) & (c) Experimental and simulated results of the monostatic radar scattering cross section for the cubes (normalised to the cross sectional area of the cube) with radiation incident at 45 degrees to the normal of the faces*

*(along the [110] vector) polarized parallel (b) and perpendicular (c) to that edge (see insets).*

The simulated and experimental results for select orientations is shown in Fig. 6, with the 3D printed samples demonstrating excellent agreement with the simulations and showing an RCS profile 15 times its geometric cross section at the dipolar resonance.

## 4. Conclusion

In conclusion, we model and experimentally characterise a new type of subwavelength microwave meta-particle scatterer, which demonstrates powerful omnidirectional scattering at its resonance and shows behaviour akin to plasmonic particles in the optical regime, with the excitation of higher order geometric modes. Samples were fabricated via additive manufacturing and metallised before characterising in an anechoic chamber. The metacubes showed a monostatic Radar cross section 15 times their geometric cross section at the dipole resonance, several times that of an equivalently sized copper cube. The quadrupole resonance showed an even stronger response, with a very narrow peak, and has potential for use in narrowband communications or unique object identifications. The metacubes are extremely light and show excellent potential for improving the radar visibility of small objects such as drones.

## 5. Acknowledgments

This work was funded by the Engineering and Physical Sciences Research Council (EPSRC), UK under a Programme Grant (EP/N010493/1) ‘‘SYnthesizing 3D METAmaterials for RF, microwave and THz applications” (SYMETA). J. G. Beadle also acknowledges support from the EPSRC and QinetiQ Ltd. via the TEAM-A prosperity partnership (Grant No. EP/R004781/1). The work of D. Cheadle and T. H. Loh were supported by the 2017 – 2020 National Measurement System Programme of the UK government’s Department for Business, Energy and Industrial Strategy (BEIS). The authors would like to thank David Knight from NPL for his work on the implementation of the measurement techniques used in the anechoic chamber.

## 6. References

1. Bogle, R. & Trizna, D. *Small Boat HF Radar Cross Sections*. Naval Res. Lab. Memo. Rept. 3322, July 1976,
2. Arbuthnot, R. S. & Badcoe, S. R. Enhancement of the radar echoing area of gliders at S- and X-bands. *Radio Electron. Eng.* **30**, 123–128 (1965).
3. Ritchie, M., Fioranelli, F., Griffiths, H. & Torvik, B. Micro-drone RCS analysis. in *2015 IEEE Radar Conference* 452–456 (IEEE, 2015). doi:10.1109/RadarConf.2015.7411926
4. Li, C. J. & Ling, H. An Investigation on the Radar Signatures of Small Consumer Drones. *IEEE Antennas Wirel. Propag. Lett.* **16**, 649–652 (2017).
5. Speretta, S. *et al.* Cubesats to Pocketqubes: Opportunities and Challenges. in *67th International Astronautical Congress (IAC)* (2016).
6. O’Malley, J. The no drone zone [airport security]. *Eng. Technol.* **14**, 34–34 (2019).
7. Jacklin, S. A. *Small-Satellite Mission Failure Rates*. NASA Technical Memo 220034 (2018).
8. Li, C., Yin, J., Zhao, J., Zhang, G. & Shan, X. The selection of artificial corner reflectors based on RCS analysis. *Acta Geophys.* **60**, 43–58 (2012).
9. Jie, G., Hong-Cheng, Y. & Qi, J. An Empirical RCS Formula of Bistatic Luneberg Lens Reflector. in *Procedia Computer Science* **147**, 97–101 (Elsevier B.V., 2019).
10. Vinogradov, S. S., Smith, P. D., Kot, J. S. & Nikolic, N. Radar cross-section studies of Spherical Lens Reflectors. *Prog. Electromagn. Res.* **72**, 325–337 (2007).
11. Briggs, J. *Target Detection by Marine Radar*. (The Institution of Engineering and Technology, 2004).
12. Ochodnicky, J., Matousek, Z., Babjak, M. & Kurty, J. Drone detection by Ku-band battlefield radar. in *2017 International Conference on Military Technologies (ICMT)* 613–616 (IEEE, 2017). doi:10.1109/MILTECHS.2017.7988830
13. Feng, M. *et al.* Wide-angle flat metasurface corner reflector. *Appl. Phys. Lett.* **113**, 143504 (2018).
14. Yau, K. S. B. Planar multi-layer passive retrodirective Van Atta array reflectors at X-band. in *2015 International Symposium on Antennas and Propagation, ISAP 2015* (Institute of Electrical and Electronics Engineers Inc., 2016).
15. Doumanis, E. *et al.* Design of engineered reflectors for radar cross section modification. *IEEE Trans. Antennas Propag.* **61**, 232–239 (2013).
16. Powell, A. W., Wincott, M. B., Watt, A. A. R., Assender, H. E. & Smith, J. M. Controlling the optical scattering of plasmonic nanoparticles using a thin dielectric layer. *J. Appl. Phys.* **113**, 184311 (2013).
17. Atwater, H. A. & Polman, A. Plasmonics for improved photovoltaic devices. *Nature Materials* **9**, 205–213 (2010).
18. Chen, X. *et al.* Broadband enhancement in thin-film amorphous silicon solar cells enabled by nucleated silver nanoparticles. *Nano Lett.* **12**, 2187–2192 (2012).
19. Wu, J. L. *et al.* Surface plasmonic effects of metallic nanoparticles on the performance of polymer bulk heterojunction solar cells. *ACS Nano* **5**, 959–967 (2011).
20. Huang, Y. & Boyle, K. *Antennas : From Theory to Practise*. (Wiley, 2008).
21. Wolff, E. *Antenna Analysis*. (John Wiley and Sons, 1966).
22. Terman, F. *Radio Engineers’ Handbook*. (McGraw-Hill Book Company, 1943).
23. Kawasaki, N. *et al.* Extinction and Scattering Properties of High-Order Surface Plasmon Modes in Silver Nanoparticles Probed by Combined Spatially Resolved Electron Energy Loss Spectroscopy and Cathodoluminescence. *ACS Photonics* **3**, 1654–1661 (2016).

24. Powell, A. W. & Smith, J. M. Mediating Fano losses in plasmonic scatterers by tuning the dielectric environment. *Appl. Phys. Lett.* **109**, 121107 (2016).
25. Wicks, M. C., Himed, B., Bracken, L. J. E., Bascom, H. & Clancy, J. Ultra narrow band adaptive tomographic radar. in *IEEE CAMSAP 2005 - First International Workshop on Computational Advances in Multi-Sensor Adaptive Processing* **2005**, 36–39 (2005).
26. NPL SMART testing chamber. Available at: https://www.npl.co.uk/products-services/radiofrequency/smart-chamber.